DOI:
10.1016/j.jconrel.2021.12.005

Document Version
Publisher's PDF, also known as Version of record

Journal of Controlled Release 341 (2022) 605–615

Contents lists available at ScienceDirect

Journal of Controlled Release

journal homepage: www.elsevier.com/locate/jconrel

Liposome delivery to the brain with rapid short-pulses of focused ultrasound and microbubbles

Sophie V. Morse [a,1], Aishwarya Mishra [b,1], Tiffany G. Chan [a,c], Rafael T. M. de Rosales [b,*], James J. Choi [a,*]

[a] Department of Bioengineering, Imperial College London, South Kensington, London SW7 2BP, UK
[b] School of Biomedical Engineering & Imaging Sciences, King's College London, St Thomas' Hospital, London SE1 7EH, UK
[c] Department of Chemistry, Imperial College London, Molecular Sciences Research Hub, White City, London W12 0BZ, UK

ARTICLE INFO

Keywords:
Focused ultrasound
Liposomes
Blood-brain barrier
Brain drug delivery
Microbubbles
Neurons

ABSTRACT

Liposomes are clinically used drug carriers designed to improve the delivery of drugs to specific tissues while minimising systemic distribution. However, liposomes are unable to cross the blood-brain barrier (BBB) and enter the brain, mostly due to their large size (*ca.* 100 nm). A noninvasive and localised method of delivering liposomes across the BBB is to intravenously inject microbubbles and apply long pulses of ultrasound (pulse length: >1 ms) to a targeted brain region. Recently, we have shown that applying rapid short pulses (RaSP) (pulse length: 5 μs) can deliver drugs with an improved efficacy and safety profile. However, this was tested with a relatively smaller 3-kDa molecule (dextran).

In this study, we examine whether RaSP can deliver liposomes to the murine brain *in vivo*. Fluorescent DiD-PEGylated liposomes were synthesized and injected intravenously alongside microbubbles. The left hippocampus of mice was then sonicated with either a RaSP sequence (5 μs at 1.25 kHz in groups of 10 ms at 0.5 Hz) or a long pulse sequence (10 ms at 0.5 Hz), with each pulse having a 1-MHz centre frequency (0.35 and 0.53 MPa). The delivery and distribution of the fluorescently-labelled liposomes were assessed by fluorescence imaging of the brain sections. The safety profile of the sonicated brains was assessed by histological staining.

RaSP was shown to locally deliver liposomes across the BBB at 0.53 MPa with a more diffused and safer profile compared to the long pulse ultrasound sequence. Cellular uptake of liposomes was observed in neurons and microglia, while no uptake within astrocytes was observed in both RaSP and long pulse-treated brains. This study shows that RaSP allows a targeted and safe delivery of liposomal drugs into the murine brain with potential to deliver drugs into neuronal and glial targets.

1. Introduction

Liposomes are the most commonly used carriers for drug delivery, enabling drugs to accumulate at a target while minimising systemic toxicity [1–4]. These drug delivery systems benefit – among other features – from high drug loading capacities, theranostic capabilities, and targeted release mechanisms (*e.g.* temperature sensitivity) [5,6]. Liposomes accumulate within organs and cells of interest *via* passive or active targeting mechanisms, and while most of the work to date has been focused on oncology, they hold great potential for the delivery of small molecule drugs for the treatment of neurodegenerative diseases [7]. However, due to their large size (~100 nm), they are unable to reach targets in the brain due to the presence of the blood-brain barrier (BBB).

The BBB is a specialized physical, transport and metabolic barrier that separates the cerebral vasculature from the parenchyma of the brain. This barrier maintains brain homeostasis, facilitating numerous functions such as ion and neurotransmitter regulation [8,9], and protects the brain by preventing neurotoxins and macromolecules from entering [10]. However, the BBB also prevents the majority of

Abbreviations: BBB, Blood-brain barrier; RaSP, Rapid Short-Pulses; DPL, DiD-PEGylated Liposomes; NOD, Normalised optical density; COV, Coefficient of variation.

* Corresponding authors.
E-mail addresses: rafael.torres@kcl.ac.uk (R. T. M. de Rosales), j.choi@imperial.ac.uk (J.J. Choi).

[1] These authors contributed equally to this work.

https://doi.org/10.1016/j.jconrel.2021.12.005
Received 9 June 2021; Received in revised form 13 October 2021; Accepted 4 December 2021
Available online 10 December 2021

therapeutic molecules from entering the brain, including 98% of small molecule drugs, thereby rendering them ineffective in the treatment of brain diseases [11].

To overcome the BBB, both invasive and non-invasive approaches have been investigated. Invasive approaches include the direct injection of agents into the brain, but this can cause neurological damage, infection, and bleeding [12]. Osmotic [13] and chemical disruption methods [14] have also been tested, but they suffer from drawbacks such as neurological damage and non-specific disruption [15], and have failed in clinical trials [16]. Other approaches, involving the modification of drugs to enable them across the BBB *via* endogenous transport mechanisms, have also been tested [17,18]. However, achieving therapeutically-relevant concentrations of these drugs in the brain remains challenging [19–22]. To increase liposome delivery to targeted regions, surface charge modifications and active molecular targeting methods – such as the conjugation of targeting vectors to the liposome's surface – have been attempted with limited success [18].

A non-invasive and targeted approach to deliver therapeutic drugs to the brain involves using focused ultrasound and microbubbles [23]. With this technique, microbubbles consisting of a lipid or protein shell and a heavy gas core (diameter 1–10 μm) are injected into the bloodstream along with the therapeutic agents of interest. Pulses of ultrasound are then applied to the targeted brain region, driving the microbubbles to oscillate, which ultimately allows the delivery of drugs across the BBB and into the brain [24,25]. *In vivo* studies have demonstrated that liposomes can be delivered into the brain using this focused ultrasound technique [26–40]. The cargo of these liposomes included genes [31,34,35], chemotherapeutics drugs [27,28,32,33,38,39] and imaging agents [29,33,36,37], with diameters ranging between 55 and 200 nm. The extent of liposome delivery has been shown to decrease as the size of the liposomes increases [37], in agreement with the protective role of the BBB towards macromolecules. Once delivered into the brain, these studies have shown heterogeneous spot-like patterns of delivery, similar to those observed with other large compounds, such as 2000 kDa (54.4 nm) dextran [41] and magnetic resonance contrast agents (1–65 nm) [42]. In terms of safety, adverse effects have been observed in many of these studies in the form of intratumoural haemorrhage, scars with infiltrating macrophages, activated astrocytes and damage to the healthy tissue surrounding tumours [26–29,33–36,38,39].

It is interesting to note that all these focused ultrasound-mediated liposomal delivery studies evaluated to date have used long-pulse sequences (~10–20 ms) emitted in a slow sequence (< 5 Hz). In recent years, a rapid short-pulse (RaSP) sequence has been developed and tested for drugs up to 3 nm in diameter [43–45]. The RaSP sequence was shown to improve the efficacy and safety of focused ultrasound-mediated drug delivery when compared to long-pulse sequences. Improvements include a more homogeneous distribution of drugs, a reduced duration of BBB permeability change (<20 min), and no tissue damage [43]. In a RaSP sequence, short pulses (in the microsecond range) are emitted at a high pulse repetition frequency in what we refer to as a burst. Each burst is then emitted at a slow rate. This sequence structure was intended to promote the spatial distribution of microbubble activity throughout the vasculature and avoid overstressing particular vessel regions [43–45]. The delivery of larger molecules such as liposomes, however, has yet to be investigated with RaSP sequences.

In this study, we evaluated whether a RaSP sequence could allow delivery of clinically-relevant PEGylated liposomes to the brain (*i.e.* same size, surface physicochemical properties, and lipid bilayer composition as Doxil/Caelyx), in comparison with a long-pulse sequence. Both efficacy and safety aspects of liposomal delivery were investigated, as well as exploring whether liposomal uptake was occurring within neurons, microglia, and astrocytes.

2. Materials and methods

2.1. Materials for liposome synthesis

For the synthesis of the liposomes, the following materials and instruments were used. Plain PEGylated liposomes (HSPC/Choline/mPEG2000-DSPE-liposomes (50:45:5 mol/mol, 100 nm) (Doxebo) were obtained from FormuMax Scientific Inc., USA as a translucent white liquid in a clear glass vial. A long alkyl chain dialkylcarbocyanine fluorescent dye DiD ($DiIC_{18}(5)$) (1,1′-Dioctadecyl-3,3,3′,3′-Tetramethylindodicarbocyanine, 4-Chlorobenzenesulfonate Salt) was obtained from Invitrogen™ as a blue solid. Size exclusion chromatography (SEC) was performed on a Superose 10/30 column (GE Healthcare Life Sciences) run at 0.5 mL/min in PBS on a GE Purifier ÄKTA FPLC (Fast Protein Liquid Chromatography). Centrifugal filtration was performed using Merck Millipore Amicon™ Ultra 100 KDa Centrifugal Filter Units in a high speed Hettich MIKRO 20 centrifuge. UV detection was performed at 214 and 280 nm. The fluorescence measurements were performed on Promega GLomax® discover system using the red excitation source at a wavelength of 644 nm with emission detected at 660–720 nm.

2.2. Synthesis of fluorescent PEGylated liposomes (DPLs)

In our design we used a DiD fluorophore to fluorescently label the PEGylated liposomes. To this end, DiD solid (2.5 mg, 2.3 μM) was dissolved in pure ethanol (1 mL) using sonication. The dye solution (3 μL) obtained was added to a Doxebo dispersion (500 μL, 60 mM lipid concentration) yielding a final DiD concentration of 15 μg/mL in the DiD/Doxebo dispersion. The DiD/Doxebo dispersion was incubated under constant rotation for 2 h at 37 °C to give DiD-PEGylated liposomes (DPLs). Free DiD solid and ethanol was removed from formed DiD-PEGylated liposomes using a PD10 minitrap G-25 size exclusion column (GE healthcare) following the manufacturer's gravity protocol. DiD-PEGylated liposomes were further purified using a 100 kDa size exclusion centrifugal filter at maximum speed. Any unattached dye that precipitated during centrifugation was separated. Dynamic light scattering (DLS) was used to study the hydrodynamic size, zeta potential and polydispersity index of the DiD-PEGylated liposomes pre- and post-DiD labelling. The incorporated dye concentration in the DPL sample was assessed by measuring fluorescence of samples at excitation wavelength of 644 nm and emission at 664 nm and compared with standard curves for the free dye signal measured in ethanol.

2.3. Serum stability of fluorescent DiD-PEGylated liposomes (DPLs)

The stability of the DiD-PEGylated liposomes in the presence of blood biomolecules was assessed to monitor dye leakage *in vitro*. The DiD-PEGylated liposomes were incubated at 37 °C in human serum ($n = 3$). At 0, 3, 12, 18, 24 and 48 h, we obtained aliquots of the serum incubated liposomes and passed them through size exclusion column of the Fast protein liquid chromatography system. 1 mL fractions from the size exclusion column were collected in PBS and UV signal was recorded. DiD-PEGylated liposomes eluted as a single peak between fractions 8 and 11, and serum proteins eluted between 18 and 25 as shown by UV signal (Fig. 2(C)). The fluorescence of all collected fractions was measured, and stability of the dye-labelled liposomes (DiD-PEGylated liposomes) was calculated as shown below:

$$\%dye\ labelled\ liposomes(stability) = \left[\frac{LF}{LF + SF}\right] * 100$$

With LF being the liposome fractions FL signal and SF being the serum protein fractions FL signal. FL is the fluorescence signal due to DiD dye associated to respective molecules at excitation wavelength of 644 nm and emission at 664 nm.

2.4. Animals and study design

Thirty-six female wild-type C57bl/6 mice (8–12 weeks old, 19.9 ± 0.6 g; Envigo, Huntingdon, UK) were used in this study. The mice were acclimatized for seven days prior to any procedure. All experimental protocols were approved by the institutional animal facility committee and the UK Home Office regulatory establishments.

Twenty-four mice were used to compare the dose and distribution of liposomal delivery in brains treated with a RaSP or long-pulse sequence at either a 0.35 or 0.53 MPa acoustic pressure with a 0 h or 2 h recovery period from the end of the ultrasound sonication ($n = 3$). These pressures were chosen in order to have a direct comparison to previous results delivering 3 kDa dextran [43]. To assess brain tissue damage, in terms of red blood cell extravasations, microvacuolations or dark neurons, an additional twelve mice were sonicated with either RaSP or long pulses at 0.35 or 0.53 MPa with no recovery time following ultrasound treatment (0 h). In all mice, the left hippocampus was treated with ultrasound while the right hippocampus was used as a no-ultrasound control. Using each animal as its own control helped reduce variabilities caused by physiological differences between animals.

2.5. Ultrasound setup and experimental conditions

Mice were anaesthetised with 1.5–2.0% vaporised isoflurane (Zoetis UK Limited, London, UK) mixed with oxygen (0.8 L/min) using an anaesthesia vaporiser (Harvard Apparatus, Cambridge, UK). The fur was first removed from the mouse's head with an electric trimmer and depilatory cream, and the head was then placed within a stereotaxic frame (45° ear bars; World Precision Instruments, Hertfordshire, UK). After applying ultrasound gel to the mouse head, a bath with a transparent parafilm membrane base was filled with degassed water and pressed onto the gel and mouse head. This helped visualise the sutures of the skull for targeting purposes. An ultrasound transducer mounted with a cone filled with distilled water and enclosed with an acoustically transparent parafilm membrane, was lowered into the water bath (Fig. 1A). For targeting purposes, a 1-mm-thick metal cross was placed at the bottom of the water bath and in alignment with the lambdoid and sagittal sutures of the skull [46]. To target the left hippocampus of the brain, the transducer was positioned 3 mm laterally from the sagittal suture, 0.5 mm anterior to the lambdoid suture and 3 mm inferior to the skull (Fig. 1B) [43]. This brain region was chosen due to the low acoustic attenuation of the parietal bone and its potential as a therapeutic target. The hippocampus is the brain's memory centre and is affected by Alzheimer's disease. The opposite right hippocampus was used as a control (no ultrasound treatment) in all experiments. For targeting, the ultrasound transducer was used in pulse-echo mode. In this mode, the transducer was connected to a pulser-receiver (DPR300; Insidix, Seyssins, France) and moved by a 3D computer-controlled positioning system (Velmex Inc., Bloomfield, NY, USA).

Once targeted, the single-element spherical-segment focused ultrasound transducer (centre frequency: 1 MHz, focal depth: 60.5 mm, diameter: 90 mm; Sonic Concepts, Bothell, WA, USA) was used to emit the therapeutic ultrasound pulses. These pulses were generated by one or two function generators (33500B Series; Agilent Technologies, Santa Clara, CA, USA) and passed through a 50-dB power amplifier (Precision Acoustics Ltd., Dorchester, UK) before reaching the transducer. A single function generator was used to emit the long-pulse sequence, while two function generators, one for the pulse shape and the other for the pulse sequence, were used to emit the RaSP sequence. Brains were exposed to either a RaSP sequence (pulse length: 5 cycles, pulse repetition frequency: 1.25 kHz, burst length: 10 ms, burst repetition frequency: 0.5 Hz) or a long-pulse sequence (pulse length: 10,000 cycles, pulse repetition frequency: 0.5 Hz). For both sequences, peak-negative pressures of 0.35 and 0.53 $MPa_{pk\text{-}neg}$ and a total of 125 pulses were emitted. The pressure amplitudes reported were measured with a needle hydrophone (needle diameter: 0.2 mm, Precision Acoustics Ltd., Dorchester, Dorset, UK) in a degassed water tank. All values were attenuated by 11.2 ± 3.2% to correct for the skull attenuation, which was measured experimentally through the parietal bone of the mouse's skull ($n = 4$) [43]. The axial, lateral and elevational full width at half maximum pressures of the ultrasound beam were 20 mm, 2 mm and 1 mm respectively.

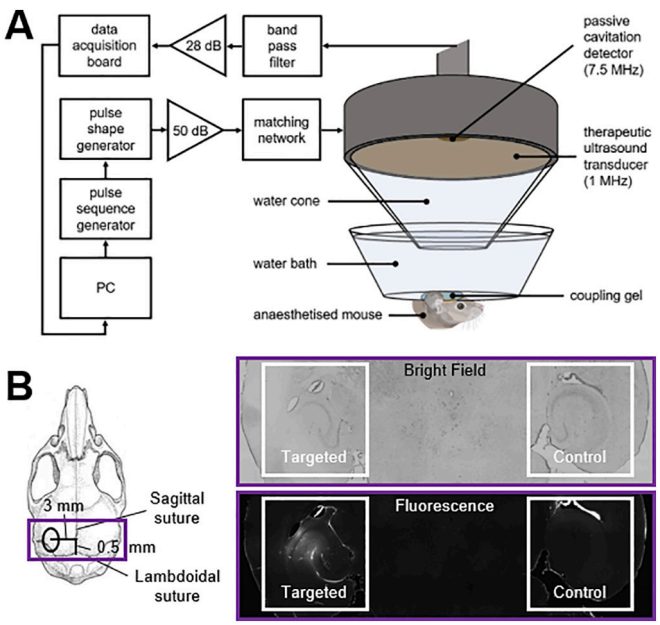

Fig. 1. Ultrasound experimental setup. (A) Ultrasound pulses were emitted from the therapeutic transducer (1 MHz) driven by one or two function generators through a 50-dB amplifier and an impedance matching network. A 7.5-MHz passive cavitation detector captured the acoustic emissions from the microbubbles, which were filtered by a band pass filter, amplified by a 28-dB pre-amplifier and recorded by a 14-bit oscilloscope. **(B)** Ultrasound was focused through the intact scalp and skull onto the left hippocampus of the mouse's brain while the right hippocampus was used as a control (no ultrasound). (PC = personal computer, dB values refer to the amount of amplification).

Acoustic emissions from the microbubbles were passively captured during the ultrasound treatment using a passive cavitation detector (PCD, centre frequency: 7.5 MHz, focal length: 76.2 mm; Olympus Industrial, Essex, UK). This detector was coaxially aligned through the rectangular central opening of the therapeutic transducer. The emissions were filtered by a 3–30 MHz band-pass filter (Mini circuits, Brooklyn, NY, USA), amplified by a 28 dB pre-amplifier (Stanford Research Systems, Sunnyvale, CA, USA) and then recorded by a 14-bit oscilloscope (GaGe model Octave Express; 100 MS/s Dynamic Signals, Lockport, IL). Time domain traces were displayed in real-time to determine whether microbubble activity was occurring during the ultrasound treatment. The acoustic emissions were processed in Matlab (Mathworks, Natick, MA, USA) to evaluate the energy levels compared to those of control pulses.

2.6. Liposomes (DPLs) and microbubble administration

Prior to the ultrasound sonication, the DiD-PEGylated liposomes (DPLs) were injected intravenously into the bloodstream through a 30 G catheter over a 30 s time-period (lipid concentration: 60.0 ± 0.9 mM, 42.6 ± 0.7 mg/mL; dye concentration: 2.1 ± 0.5 μg/mL). Ten seconds into the ultrasound sonication – allowing five control pulses to be emitted – SonoVue® microbubbles (Bracco, Milan, Italy) were injected through the same catheter over a 30 s time period (concentration: 5 μL/g of body mass, vial concentration: 3×10^8/mL). The microbubbles were activated following manufacturers' instructions and used within 6 h from activation.

2.7. Histological staining

The mice were euthanised *via* transcardial perfusion, either immediately or 2 h after the end of the ultrasound sonication, with 20 mL ice-cold PBS with added heparin (20 units/mL) and 20 mL 10% formalin (Sigma Aldrich, St Louis, MO, USA). The brains were extracted, fixed in formalin overnight, followed by 30% sucrose overnight for cryoprotection. Once embedded in optimal cutting temperature compound (OCT; Agar Scientific, Stansted, UK), the brains were sectioned into sixty 30 μm slices to cover the entire hippocampus using a cryostat (CryoStar NX70; Thermo Fisher, Waltham, MA, USA).

Immunostaining was performed on the brain slices where cellular uptake of the liposomes was observed to determine whether they were being uptaken by neurons, microglia or astrocytes. Neurons were stained using a primary recombinant anti-NeuN antibody (1:500 overnight; Ab177487; Abcam, Cambridge, England) and a secondary goat anti-rabbit IgG H&L Alexa Fluor® 488 antibody (1:500 for 2 h; Ab150077; Abcam). Microglia were stained using a primary anti-Iba1 antibody (1:500 overnight; Ab5076; Abcam) and a secondary donkey anti-goat IgG H&L Alexa Fluor® 488 antibody (1:500 for 2 h; Ab150129; Abcam). Astrocytes were stained using a primary GFAP monoclonal antibody (1:50 overnight; 13-0300; ThermoFisher) and a secondary mouse anti-rat IgG2a FITC antibody (1:500 for 2 h; 11-4817-82; ThermoFisher). No statistical analysis was performed on our cellular uptake data due to the limited number of brain slices with cellular uptake for each type of cell staining.

To assess tissue damage, a set of twelve brains (treated with RaSP or long pulses, at 0.35 or 0.53 MPa) were sent to IQPath laboratory at University College London to be paraffin-embedded and sectioned into 6 μm thick slices. With 1.5 mm discarded from the dorsal side of the brain, eleven levels with six sections each were cut, with 80 μm of tissue discarded between levels. The first side of each level was stained with H&E.

2.8. Microscopy and analysis

Images of the liposome delivery and the antibody staining were acquired using fluorescence microscopy (10×; Zeiss Axio Observer; Oberkochen, Germany) and confocal microscopy (20×; Zeiss LSM-510 inverted; Oberkochen, Germany). The DiD fluorophore, which was incorporated in our liposome formulation to localise them fluorescently, was excited at 640/30 nm and emissions were filtered at 690/50 nm. To detect neurons, microglia and astrocytes, Alexa Fluor 488 and FITC-labelled antibodies were used to stain the brain slices and they were excited at 470/40 nm and emissions were filtered at 525/50 nm.

The amount of fluorescence detected was measured with the normalised optical density (NOD) [47]: pixels with intensities higher than the mean of the control region plus twice its standard deviation were summed for both the control and targeted regions of interest. The sum of the targeted region was subtracted by that of the control region to obtain the NOD. The distribution of the probes was quantified with the coefficient of variation (COV), defined as the standard deviation over the average fluorescence intensity in the targeted region. This was calculated for six slices for each treated brain by selecting regions of interest around the targeted left hippocampus using Matlab® (2016a, The Mathworks, Natick, MA, USA). The COV calculation was only performed on brains that displayed liposomal delivery.

To determine the number of spot-like areas of liposomal delivery, the number of areas above 100 μm^2 was quantified (as shown in [29]). Larger areas of delivery were expected if the liposomes diffused further away from the blood vessels. Regions of interest were selected around all spots of liposome delivery in six sections per brain. An automatic threshold was applied equally to all images in ImageJ (dark triangle) to only select regions of liposome delivery. The area of each region was determined by using the automated 'Analyse Particles' tool in ImageJ [48].

Seven H&E-stained sections per brain were blindly assessed for tissue damage with three histological measures evaluated: the number of sites with more than five red blood cells extravasated, the number of microvacuolations, and the number of dark neurons.

2.9. Statistical analysis

A one-way analysis of variance (ANOVA) test was conducted to assess whether differences were present between the parameter sets in the NOD, COV and areas above 100 μm^2 results. *Post hoc* Bonferroni analysis was performed to estimate any significant differences in a pairwise manner ($P < 0.05$). A Wilcoxon rank sum test was performed to test whether difference between the H&E results were significant. All analysis was carried out in Matlab R2019b.

3. Results

3.1. Synthesis and characterization of the fluorescent DiD-PEGylated liposomes (DPLs)

The Doxebo liposomes (empty PEGylated liposomes) were labelled with DiD (1,1′-Dioctadecyl-3,3,3′,3′-tetramethylindodicarbocyanine, 4-Chlorobenzenesulfonate Salt), a far-red fluorescent, lipophilic and cationic indocarbocyanine dye used to stain phospholipid bilayers (Fig. 2A) [49]. This labelling process showed negligible changes of the hydrodynamic diameter (pre-DiD: 99.9 ± 3.6 nm *vs.* post-DiD: 97.9 ± 2.2 nm) and no effect on surface charge (Fig. 2B), compared to the original Doxebo liposomes. The hydrodynamic size of the liposomes and their polydispersity remained stable following labelling (Fig. 2B). Using a fluorescence standard curve, we calculated that the DiD concentration in the final DPL sample was 2.1 ± 0.5 μg/mL.

It has been shown that lipoproteins in blood serum can cause fluorescent dyes to leak from liposomes *via* lipids passively dissociating from the bilayers of the liposomes [50]. To assess whether DiD was retained in the liposomes in the presence of blood components, we incubated a small amount of DPLs *in vitro* with a large excess of human serum at 37 °C for up to 48 h, and used size-exclusion chromatography to detect dye leakage. Using this system, both DPLs and serum components were efficiently separated, identified, and quantified *via* UV and fluorescence measurements allowing us to determine the liposome and serum protein-associated dye eluted at different timepoints (Fig. 2C). Co-elution of the liposomes (as measured by UV) and the incorporated dye (from fluoresce detection) over time under these conditions demonstrate high stability of the dye within the liposomes for up to 48 h (Fig. 2D).

3.2. Ultrasound-mediated liposomal delivery to the brain

To investigate whether focused ultrasound emitted in a rapid short-pulse sequence (RaSP) could deliver these liposomes into the brain, we sonicated the left hippocampus of mice with either a RaSP or a long-pulse sequence while intravenously injecting microbubbles. Brains were treated with one of two acoustic pressures (0.35 or 0.53 MPa) and extracted either 0 or 2 h after the ultrasound treatment.

Liposome fluorescence was detected in brains treated with RaSP and long-pulse sequences (Fig. 3). With RaSP, delivery was only observed in brains treated with the higher acoustic pressure (0.53 MPa), while with long pulses, delivery was observed at both pressures. However, with long pulses at the lower 0.35 MPa pressure (0 h), delivery was only detected in two thirds of the brains treated. As expected, no fluorescence was detected in the control right hippocampi of all brains.

A higher fluorescence signal (greater liposomal delivery) was detected with long pulses compared to RaSP and also at the higher acoustic pressure compared to the lower one, which was confirmed by calculating the normalised optical density (NOD; Fig. 4A). Interestingly, a higher fluorescence was detected on average with RaSP at 0.53 MPa

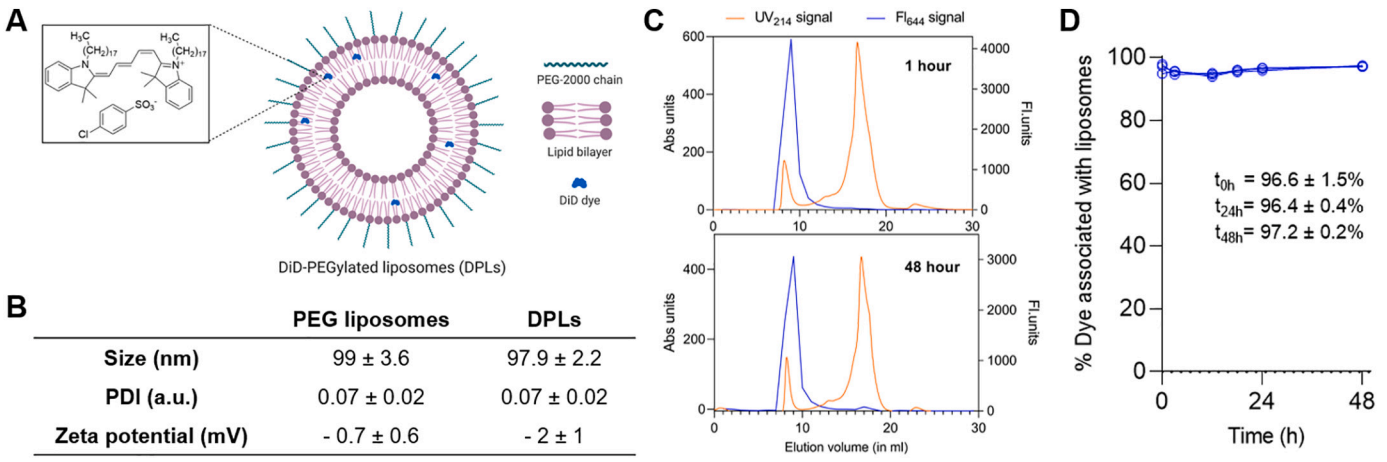

	PEG liposomes	DPLs
Size (nm)	99 ± 3.6	97.9 ± 2.2
PDI (a.u.)	0.07 ± 0.02	0.07 ± 0.02
Zeta potential (mV)	- 0.7 ± 0.6	- 2 ± 1

Fig. 2. DiD-PEGylated liposomes (DPLs). (A) The carbocyanine dye DiD is incorporated in the phospholipid bilayer of the PEGylated liposome due to its hydrophobic nature. **(B)** The hydrodynamic size distribution polydispersity index (PDI, measure of size distribution), and zeta potential of the PEGylated liposomes show negligible changes ($n = 4$) before and after incorporation of the dye. **(C)** Size exclusion chromatograms show the stability of the DPLs (fluorescent liposomes) post incubation in human serum and 37 °C for up to 48 h and confirm a high retention of the dye within the liposomes. Fractions 8–10 contained the liposomes and fractions 12–25 contained the serum proteins. The high fluorescence signal in fractions 8–10 at both timepoints confirmed the retention of DiD in the liposomes up to 48 h. **(D)** Serum stability curve shows % dye associated with the liposomes post incubation in serum at time points 0, 3, 12, 18, 24, 48 h.

compared with long-pulse treatments at 0.35 MPa. The two-hour recovery time created a significant difference in the NOD only with long pulses at 0.35 MPa ($P < 0.05$).

3.3. Liposome distribution

Liposomes were found to distribute heterogeneously within the targeted area of all brains (Fig. 3), with sites of delivery mostly concentrated around blood vessels. The distribution was quantified using the coefficient of variation (COV), which is defined as the standard deviation over the average fluorescence intensity in the targeted region. The COV showed that there was less variation in the distribution of the liposomes in RaSP-treated brains (Fig. 4B), indicating a more uniform distribution in the delivery, which was found to be less densely concentrated around the blood vessels.

To determine whether there were differences in the number and size of regions with liposome delivery between the different parameters sets tested, the number of areas above 100 μm^2 and their average size was quantified. The number of areas was higher with long pulses compared to RaSP and increasing the acoustic pressure led to an increase in the number of delivery sites (Fig. 4C). Allowing 2 h for the liposomes to extravasate into the brain and diffuse within the parenchyma only lead to significant differences in distribution with long pulses at 0.35 MPa. The average size of the areas above 100 μm^2 showed no significant differences between brains (Fig. S1).

3.4. Subcellular localisation and cellular uptake

Within the targeted left hippocampus, the delivered liposomes were distributed throughout the parenchyma and were also uptaken by cells with both sequences. Confocal microscopy images showed that the fluorescence signal was localised in the cytoplasm and was not found within the nucleus (Fig. 5). The fluorescence within the cytoplasm was heterogenous with a spot-like distribution.

Immunohistochemical staining was performed to determine which brain cells were taking up the delivered liposomes. Uptake was confirmed within neurons (Fig. 6A-B) and in microglia (Fig. 6C-D), while no uptake was observed within astrocytes (Fig. 6E-F). In both neurons and microglia, the degree of uptake was found to be higher in long-pulse treated brains compared with RaSP-treated brains.

3.5. Tissue damage

H&E staining was performed to assess whether any tissue damage was caused by RaSP or long-pulse treatments at 0.35 and 0.53 MPa (0 h; Fig. 7A-Z). No tissue damage was observed in RaSP-treated brains at both pressures (Fig. 7A-C, G-I, M-O, S-U, Y-Z), with the exception of a single site of red blood cell extravasation in one brain at the higher acoustic pressure (Fig. 7O). On the other hand, with long-pulses, tissue damage in the form of red blood cell extravasations, microvacuolations and dark neurons was observed in all brains (Fig. 7D-F, J-L, P-R, V-X, Y-Z). These sites of damage were found to be larger at the higher 0.53 MPa pressure.

4. Discussion

In this study we have shown that clinically-relevant PEGylated liposomes of approximately 100 nm in diameter can be delivered to the brain when emitting rapid short-pulses (RaSP) of focused ultrasound. Based on our H&E analysis, there was no detectable damage produced by RaSP emissions. To the best of our knowledge, this is the first demonstration of liposome delivery with short ultrasound pulses as previous studies have used long-pulse sequences [26–39].

The DPLs synthesized for this study are constituted of two key components chosen due to their favourable properties. The doxorubicin-free PEGylated nano-liposomes (Doxebo) were chosen due to their similarity to the clinically used liposomes, Doxil/Caelyx. The dye DiD used for labelling Doxebo has a high fluorescence and photostability in lipid environments and weak fluorescence in aqueous medium, allowing us to detect only the encapsulated dye and not the free dye. DiD labelling has been shown by others to be a robust method with very low leakage from lipid bilayer membranes over long time periods, while maintaining the physicochemical properties of the nanoparticles [50,51], and our results are in agreement with these findings. Our data showing that DPLs did not show any changes in their physicochemical properties after labelling, and the high label retention make DPLs excellent candidates for studying these drug-delivery vehicles *in vivo*.

To investigate whether DPLs could be delivered with RaSP within a similar acoustic pressure range to previous long-pulse studies (Supplementary Table 1), liposomal delivery was tested at 0.35 and 0.53 MPa. With RaSP, a higher acoustic pressure (0.53 MPa) was required to achieve delivery, indicating a higher-pressure threshold for liposomal delivery compared to that required for long pulses. When comparing

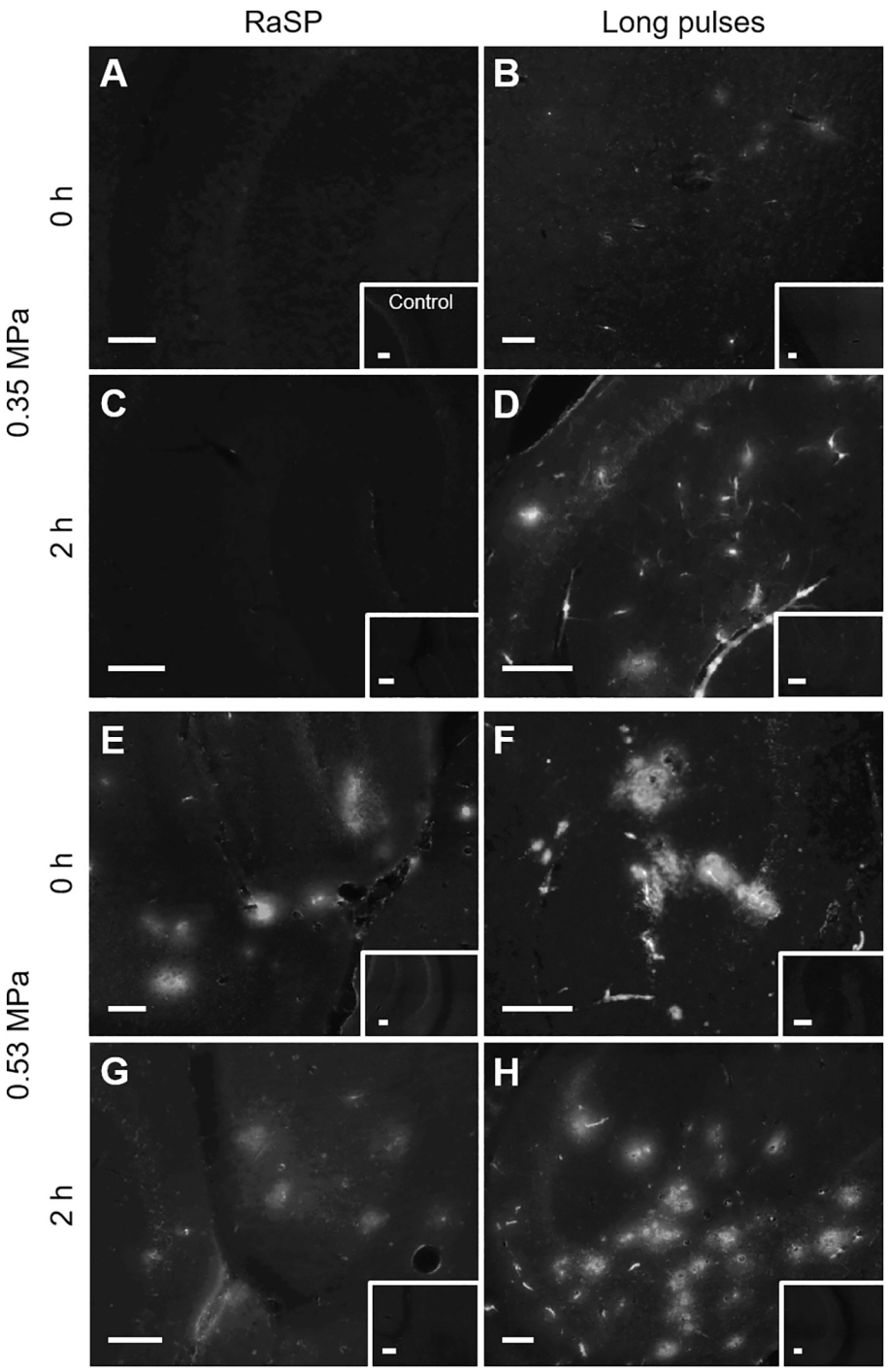

Fig. 3. Liposomal delivery with rapid short-pulse (RaSP) and long-pulse sequences at 0.35 and 0.53 MPa, at 0 h or 2 h after ultrasound treatment. Fluorescence images (10×) show examples of liposomes delivered with **(A, C, E, G)** RaSP and **(B, D, F, H)** long-pulse sequences at **(A-D)** 0.35 MPa and **(E-H)** 0.53 MPa, at either **(A-B, E-F)** 0 h or **(C-D, G-H)** 2 h after the ultrasound treatment. Right hippocampus control regions are shown in white boxes in the bottom right corner of each image. **(A, C)** No delivery was observed at 0.35 MPa when brains were treated with a RaSP sequence and in one third of the brains treated with long pulses. **(E-H)** At 0.53 MPa, delivery was observed in all brains. More spots of delivery were observed in long-pulse compared to RaSP-treated brains. The white scale bars indicate 50 μm.

results at equivalent acoustic pressures, the fluorescence detected from the delivered fluorescent liposomes was lower with RaSP compared to long-pulse-treated brains (Figs. 3–4). These results were expected given that 150 times less acoustic energy is deposited in the brain with RaSP. We also hypothesise that the low-energy short pulses emitted in the RaSP sequence will stimulate gentler microbubble oscillations, leading to a lower extravasation of these large liposomal agents into the brain.

An increase in the pressure amplitude led to an increase in liposomal delivery, both in terms of the overall detected fluorescence and the number of delivery regions (Fig. 4). These results were also expected as previous studies with long pulses have shown that higher pressures increase the magnitude of the BBB permeability enhancement [29,41,47,52,53], thereby increasing not only the delivery of liposomes [29], but also the delivery of high molecular weight dextran molecules (70 and 2000 kDa) into the brain [41].

Differences in the extent of agent delivery have also been observed previously depending on the amount of time these delivered agents are given to extravasate and diffuse within the brain. Other groups have investigated liposomal delivery at 0, 2 and 4 h after ultrasound exposure [29,31,36]. Here, we explored liposomal delivery at 0 and 2-hour timepoints and found that only with long pulses at 0.35 MPa, the detected fluorescence and number of delivery spots was significantly different between brains at the two timepoints (Fig. 4). These results could be explained by the longer increase in BBB permeability found with long pulses compared with RaSP [43], which would allow liposomes to extravasate into the brain for longer periods of time. In the

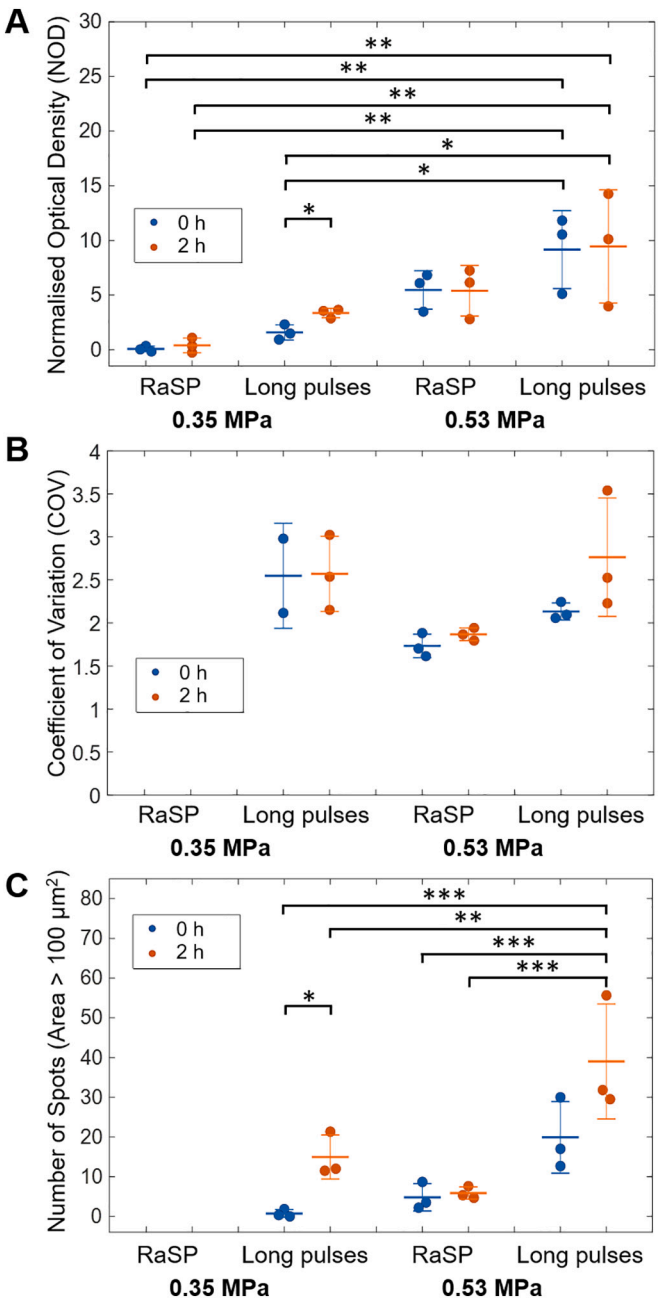

Fig. 4. Detected dose, distribution, and number of delivery sites with rapid short-pulse (RaSP) and long-pulse sequences at 0.35 and 0.53 MPa, and at 0 h or 2 h after ultrasound treatment. (A) The threshold for liposomal delivery with RaSP was found to be between 0.35 and 0.53 MPa, quantified with the normalised optical density (NOD). No delivery was detected in RaSP brains at 0.35 MPa and only in one third of long-pulse brains at this lower pressure. **(B)** A lower coefficient of variation (COV) was found in RaSP-treated brains compared to in long-pulse-treated brains, indicating less variation and a more homogeneous distribution. The COV was not quantified in brains where no liposomal delivery was observed. **(C)** The number of areas above 100 μm^2 with liposome delivery was found to be higher in long-pulse compared to RaSP-treated brains with the same acoustic pressure. Increasing the acoustic pressure led to a higher number of delivery regions in both RaSP and long-pulse-treated brains. Waiting 2 h post-sonication also led to an increase, but only in long-pulse treated brains at 0.35 MPa. The areas were not quantified when no liposomal delivery was observed. * = $P < 0.05$, ** = $P < 0.01$ and *** = $P < 0.001$.

other brains, the lack of significant differences when waiting 2 h could be explained by the limited diffusion of these 100 nm liposomes through the nearly 64 nm pores of the extracellular matrix [54].

The distribution pattern of the delivered liposomes was found to be heterogenous with both sequences, characterised by distinct spots of delivery with cloud-like peripheries (Fig. 3). This finding was consistent with previous studies that have shown heterogenous patterns of liposome delivery with long pulses [29,31,32,36]. This pattern suggests a confined diffusion of the liposomes within the extracellular matrix following their extravasation from the blood vessels into the brain. This is likely due to the slow diffusion of these large agents through the width of the extracellular matrix pores as mentioned above [54]. However, liposomes are designed to carry much smaller drugs and imaging agents, such as doxorubicin (~ 2 nm diameter [55]), which would be released into the brain once the liposomes have crossed the BBB. Therefore, it is these smaller agents that would be required to diffuse throughout the brain parenchyma to reach target sites, rather than the liposomes themselves. A more homogeneous distribution of the liposomes would facilitate a more uniform spread of the loaded drug; however, it is yet to be investigated whether this is essential. In RaSP-treated brains a slight – though not significant – decrease was observed in the heterogeneity of liposome delivery based on the COV quantification (Figs. 3–4). Qualitatively, a more uniform drop in the fluorescence intensity values from the blood vessels was observed, which we hypothesise could be due to a gentler enhancement in the BBB permeability with RaSP.

The delivered liposomes were not only found to distribute throughout the targeted brain parenchyma but were also taken up by cells. Knowing that this ultrasound delivery technique allows liposomes to reach areas where brain cells are present is of interest, as liposomes can be functionalised to bind to specific receptors expressed by brain cells. We therefore investigated whether liposomes were reaching neurons, microglia and astrocytes, which are important targets for therapeutic and neuroprotective drugs as well as imaging agents, and which, in the case of the glial cells, could indicate a pathway of liposome excretion.

Neuronal uptake of the liposomes was observed with both pulse sequences with higher uptake in long-pulse-treated brains, which we hypothesise is due to the higher number of delivery sites (Fig. 4). Without an ultrasound delivery system, liposome uptake in neurons has previously been observed *in vitro* [56–59] and *in vivo* using invasive delivery procedures [58–60]. With focused ultrasound, liposome uptake within neurons can be achieved non-invasively. Within the neurons, liposomes were detected throughout the cytoplasm in a spot-like distribution and not in the nucleus. This distribution has been previously reported with both cationic and anionic liposomes [57–59] and it suggests that the liposomes are being taken up within lipid-rich compartments in the cytoplasm, such as endosomes or lysosomes. Future staining for these lipid compartments could provide insight into the pathway of uptake and excretion of these liposomes from neurons.

Liposome uptake was also observed within microglia, which represent the primary defence system of the brain. Previous studies without ultrasound have shown that targeted and untargeted liposomes can be uptaken by microglia, with varying results depending on the liposomal composition [61–63]. In our experiments, uptake was only observed at the higher pressure (0.53 MPa) and 2 h after the ultrasound treatment, with higher uptake in long-pulse treated brains compared with RaSP. We hypothesise that these results are due to the higher number of liposome delivery sites at the higher pressure and when using the long pulses compared with the RaSP. In addition, the more disruptive microbubble activity induced by the long pulses and higher pressures could be eliciting more phagocytic activity in the microglia compared to the RaSP treatment, leading to liposome uptake in microglia as a method of excretion from the brain. The fact that microglial uptake is only observed at the two-hour timepoint is not surprising given that microglial response often requires time to manifest [64,65]. This could also be due to the slow extravasation of these liposomes into brain regions

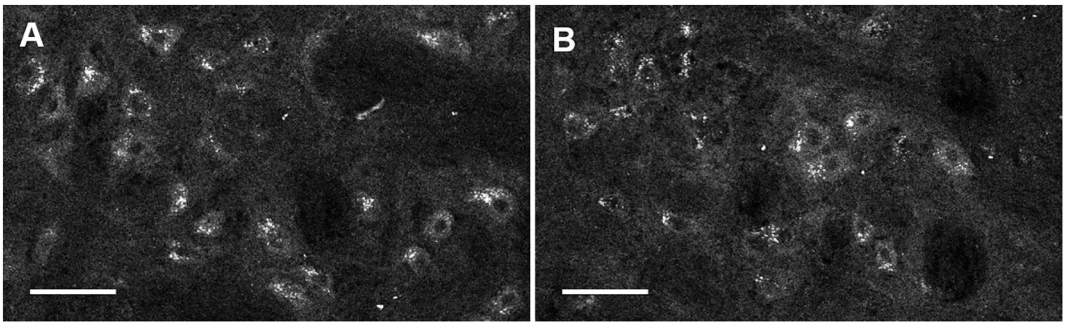

Fig. 5. Subcellular localisation of liposomes. (A-B) Two representative confocal images (20×) showing details of the subcellular localisation of the liposomes (white) within ultrasound-targeted regions of long-pulse treated brains at 0.53 MPa two hours after the ultrasound treatment. Fluorescence was observed within the cells, specifically in the cytoplasm and not in the nucleus (darker circular centre within the cells). The scale bars indicate 50 μm.

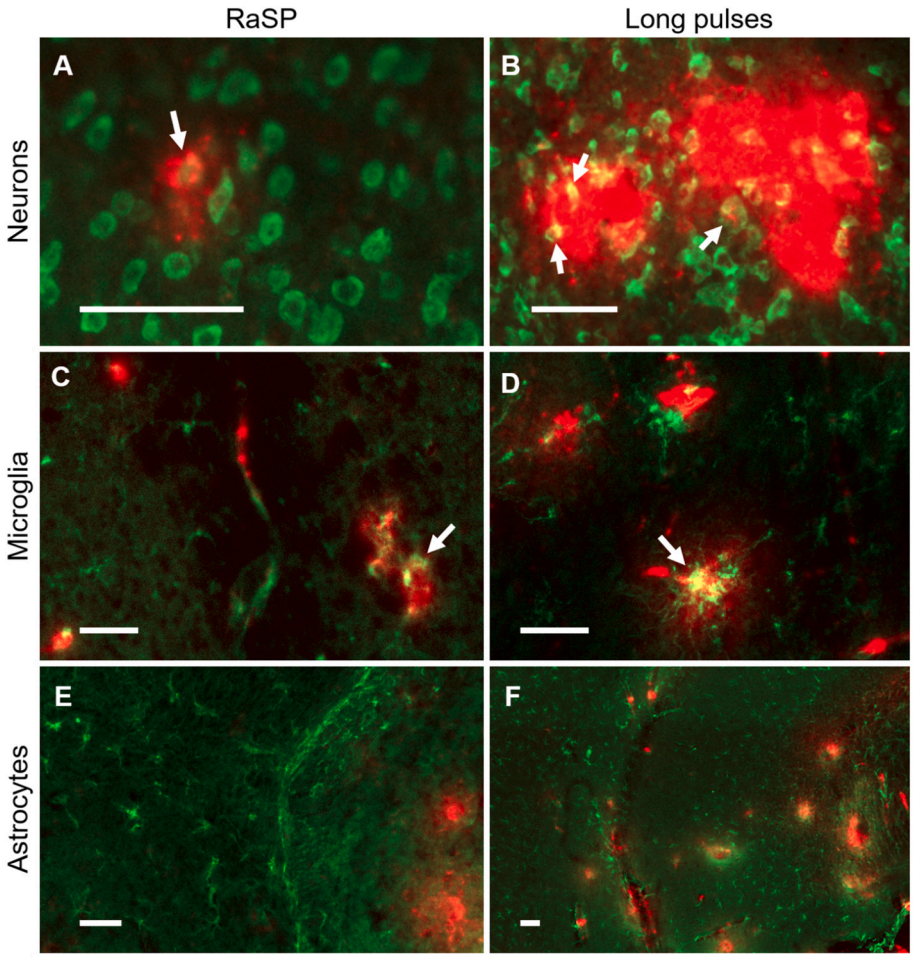

Fig. 6. Cellular uptake of liposomes within neurons and microglia but not in astrocytes in RaSP and long-pulse treated brains. Fluorescence images (10×) show whether liposomes (red) were taken up by **(A-B)** neurons (NeuN, green), **(C-D)** microglia (Iba1, green) and **(E-F)** astrocytes (GFAP, green). **(A-B)** Uptake within neurons was observed with both sequences in all brains, though higher uptake was seen in long-pulse treated brains. **(C-D)** Uptake within microglia was only observed at 0.53 MPa 2 h after the ultrasound treatment with both RaSP and long-pulses, with higher uptake in long-pulse treated brains. **(E-F)** No liposome uptake was observed in astrocytes in all brains. White arrows highlight examples of liposome uptake within neurons and microglia. The scale bars indicate 50 μm. (For interpretation of the references to colour in this figure legend, the reader is referred to the web version of this article.)

where the microglia are located, as well as the properties of the liposomes themselves, in terms of size and biocompatibility for immune response recognition. Future work will focus on determining quantitatively whether the microglia uptaking the liposomes are in an activated state, in order to gain a better understanding of the microglial response to this type of treatment.

No liposome uptake was observed in astrocytes with both pulse sequences. Previous studies have only shown astrocyte uptake when the liposomes were targeted to these cells and *in vitro* [66–68]. The BBB is thought to be the main reason why targeted liposomes have failed to reach astrocytes in experiments. Future work should investigate whether uptake in astrocytes occurs at later time points since astrocytes have been shown to react later than microglia [69,70]. In addition, staining could determine whether any of the astrocytes have become reactive.

With RaSP, an improved safety profile was observed at both the lower and higher pressures (0.35 and 0.53 MPa) compared to brains treated with long pulses. Indeed, no damage was observed in any of the brains with RaSP, except for a single site of red blood cell extravasation at the higher pressure. On the other hand, our long-pulse results reflect findings from other studies [29,35,36,52,53], with larger sites of tissue damage at the higher pressure thought to be caused by higher magnitudes of cavitation. A safer and gentler sonication would be preferred to avoid unnecessary disruption of any healthy tissue, for example, at

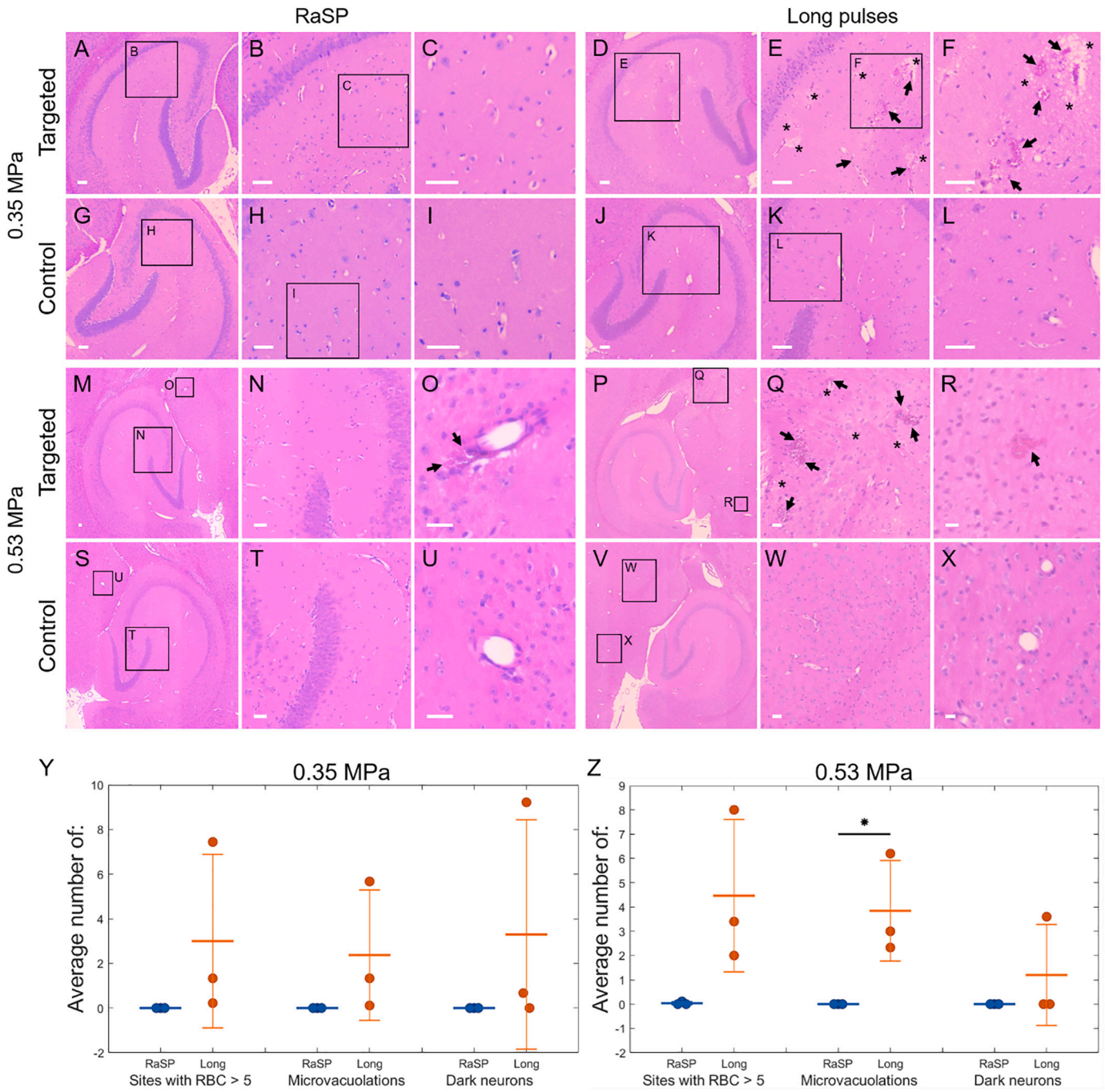

Fig. 7. Tissue damage assessment in RaSP and long-pulse treated brains at 0 h. (A-I, M-U) H&E staining showed no tissue damage in all RaSP-treated brains at both pressures (0.35 and 0.53 MPa) except for a **(O)** single small site of red blood cell extravasation at the higher pressure. **(D-L, P-X)** Histological damage was observed at multiple sites within the ultrasound targeted area in all brains treated with long pulses: red blood cell extravasation (arrows), microvacuolations (asterisks) and dark neurons. The black boxes show enlarged regions displayed on the right-hand side of each image. The scale bars indicate 50 μm.

tumour margins or in tissue we would like to repair (*e.g.*, Alzheimer's disease). Future work will investigate safety at later time points.

Although a higher pressure was required to achieve liposome delivery with the RaSP sequence, an improved safety profile was obtained as well as a higher delivery efficacy compared with long pulses at the lower pressure. In addition, there is scope to optimise this RaSP sequence further for the delivery of these 100 nm liposomes as the parameters used to date are those with which we have shown the efficient and safe delivery of 3 kDa dextran [43].

Future work will focus on investigating whether therapeutically relevant concentrations of drugs carried by these liposomes can be reached in the brain with RaSP. We will explore the efficacy of liposomal drug release in tumour environments, establishing how differences in permeability, interstitial pressure and vasculature heterogeneity affect drug delivery patterns compared to healthy brain tissue [71,72]. In addition, the effect of ultrasound and microbubbles on possible increased drug release will be studied *in vitro*. Previous work has shown that ultrasound can trigger drug release from liposomes, however, most of these studies used either thermally sensitive liposomes in combination with high intensity focused ultrasound or injected liposomes attached to the microbubbles to encourage their release during the microbubble oscillations [73–75].

Based on our results, we believe that the selection of RaSP *vs.* long pulses for drug delivery will depend on various factors including the size and circulation time of the drug being delivered, and the targeted disease. If the drug has long circulation times, such as the PEGylated liposomes used here, long pulses that induce BBB opening for long periods of time seem logical and may be beneficial to improve the delivered dose, but at the expense of an increasing safety risk due to the length of time the BBB remains open. This risk, however, needs to be balanced with the aggressiveness of the disease, its stage, and its location; for example, when treating an aggressive late-stage brain tumour. RaSP sequences, on the other hand, result in shorter BBB opening times (<20 min) and lower tissue damage that may be applicable to both short and long circulating drugs. Example applications may include when the targeted disease requires repeated deliveries, when the targeted region of diseased tissue is in close proximity to healthy tissue (*e.g.* neurodegenerative diseases) or at the margins of less aggressive or early-stage brain tumours.

5. Conclusions

In this study, we have shown that rapid short ultrasound pulses (RaSP) enable the delivery of 100 nm PEGylated liposomes into the brain. The RaSP sequence at both acoustic pressures provided a safer delivery while achieving higher delivery efficacy compared to the long pulse treatments at the lower pressure. A higher acoustic pressure was required to deliver liposomes across the BBB with RaSP. Using microscopy methods, we assessed the liposomal uptake at the cellular level. Liposomes were taken up by neurons to a lower degree with RaSP than with long pulses, and were localised in the cytoplasm. Varying microglial uptake was observed with different sequences while no astrocyte uptake was detected. Lower glial cell involvement was observed in RaSP compared to long-pulse-treated brains. This improved safety profile and efficacy shows the ability of the RaSP sequence to deliver large molecules to the brain without causing damage and can be harnessed to deliver 100 nm nanoparticles to treat CNS diseases. The study of liposomal uptake at the neuronal level should improve our ability to deliver drugs to cellular therapeutic targets in the brain.

Acknowledgements

This study was funded by the Alzheimer's Research UK (ARUK-IRG2017A-7) and the PhD studentships of S.V.M., A.M. and T.G.C. funded by the King's College London and Imperial College London EPSRC Centre for Doctoral Training in Medical Imaging (EP/L015226/1) and the EPSRC Centre for Neurotechnology (EP/L016737/1). A.M and R.T.M.R also acknowledge support from EPSRC programme grants EP/S032789/1 and EP/R045046/1. This study used equipment from the Facility for Imaging by Light Microscopy (FILM) at Imperial College London, supported by funding from the Wellcome Trust (grant 104931/ZS/14/Z) and BBSRC (grant BB/L015129/1), and a Wellcome Trust Multiuser Equipment Grant at King's College London [212885/Z/18/Z]. We also acknowledge support from the Wellcome/EPSRC Centre for Medical Engineering [WT/203148/Z/16/Z] and the KCL and UCL Comprehensive Cancer Imaging Centre funded by CRUK and EPSRC in association with the MRC and DoH (England). The authors finally acknowledge support from the National Institute for Health Research (NIHR) Biomedical Research Centre based at Guy's and St Thomas' NHS Foundation Trust and KCL [grant number IS-BRC-1215-20006]. The views expressed are those of the authors and not necessarily those of the NHS, the NIHR or the Department of Health. The authors would also like to thank Hee Seok Jung and Javier Cudeiro Blanco for their help.

Declaration of Competing Interest

The authors have declared that no competing interests exist.

Appendix A. Supplementary data

Supplementary data to this article can be found online at https://doi.org/10.1016/j.jconrel.2021.12.005.

References

[1] J. Shi, P.W. Kantoff, R. Wooster, O.C. Farokhzad, Cancer nanomedicine: progress, challenges and opportunities, Nat. Rev. Cancer 17 (2017) 20–37.
[2] B. Ozbakir, B.J. Crielaard, J.M. Metselaar, G. Storm, T. Lammers, Liposomal corticosteroids for the treatment of inflammatory disorders and cancer, J. Control. Release 190 (2014) 624–636.
[3] U. Bulbake, S. Doppalapudi, N. Kommineni, W. Khan, Liposomal formulations in clinical use: an updated review, Pharmaceutics 9 (2017) 12.
[4] T.M. Allen, P.R. Cullis, Liposomal drug delivery systems: From concept to clinical applications, Adv. Drug Deliv. Rev. 65 (2013) 36–48.
[5] G.A. Koning, G. Storm, Targeted drug delivery systems for the intracellular delivery of macromolecular drugs, Drug Discov. Today 8 (2003) 482–483.
[6] J.M. Metselaar, G. Storm, Liposomes in the treatment of inflammatory disorders, Exp. Opin. Drug Deliv. 2 (2005) 465–476.
[7] S. Mukherjee, V.S. Madamsetty, D. Bhattacharya, S. Roy Chowdhury, M.K. Paul, A. Mukherjee, Recent advancements of nanomedicine in neurodegenerative disorders theranostics, Adv. Funct. Mater. 30 (2020) 2003054.
[8] P. Rutecki, Ions in the brain: normal function, seizures, and stroke, Neurology 66 (2006) 618.
[9] N.J. Abbott, L. Rönnbäck, E. Hansson, Astrocyte–endothelial interactions at the blood–brain barrier, Nat. Rev. Neurosci. 7 (2006) 41–53.
[10] M.B. Gingrich, S.F. Traynelis, Serine proteases and brain damage – is there a link? Trends Neurosci. 23 (2000) 399–407.
[11] W.M. Pardridge, The blood-brain barrier: bottleneck in brain drug development, NeuroRX 2 (2005) 3–14.
[12] R.A. Kroll, E.A. Neuwelt, Outwitting the blood-brain barrier for therapeutic purposes: osmotic opening and other means, Neurosurgery 42 (1998) 1083–1099.
[13] E.A. Neuwelt, E.P. Frenkel, J.T. Diehl, K.R. Maravilla, L.H. Vu, W.K. Clark, S. I. Rapoport, P.A. Barnett, S.A. Hill, S.E. Lewis, A.L. Ehle, C.W. Beyer, R.J. Moore, Osmotic blood-brain barrier disruption: a new means of increasing chemotherapeutic agent delivery, Trans. Am. Neurol. Assoc. 104 (1979) 256–260.
[14] R.L. Dean, D.F. Emerich, B.P. Hasler, R.T. Bartus, Cereport® (RMP-7) increases carboplatin levels in brain tumors after pretreatment with dexamethasone, Neuro-Oncology 1 (1999) 268–274.
[15] S.I. Rapoport, W.R. Fredericks, K. Ohno, K.D. Pettigrew, Quantitative aspects of reversible osmotic opening of the blood-brain barrier, Am. J. Physiol. Integr. Comp. Physiol. 238 (1980) R421–R431.
[16] M.D. Prados, S.C. Schold, H.A. Fine, K. Jaeckle, F. Hochberg, L. Mechtler, M. R. Fetell, S. Phuphanich, L. Feun, T.J. Janus, K. Ford, W. Graney, M. Prados, Neuro-Oncology A Randomized, Double-Blind, Placebo-controlled, Phase 2 Study of RMP-7 in Combination with Carboplatin Administered Intravenously for the Treatment of Recurrent Malignant Glioma 1, 2003.
[17] W.M. Pardridge, Blood-brain barrier drug targeting: the future of brain drug development, Mol. Interv. 3 (2003).
[18] D.B. Vieira, L.F. Gamarra, Getting into the brain: liposome-based strategies for effective drug delivery across the blood–brain barrier, Int. J. Nanomedicine 11 (2016) 5381–5414.
[19] C.A. Lipinski, F. Lombardo, B.W. Dominy, P.J. Feeney, Experimental and computational approaches to estimate solubility and permeability in drug discovery and development settings, Adv. Drug Deliv. Rev. 64 (2012) 4–17.
[20] V.A. Levin, Relationship of octanol/water partition coefficient and molecular weight to rat brain capillary permeability, J. Med. Chem. 23 (1980) 682–684.
[21] E.G. Chikhale, K.Y. Ng, P.S. Burton, R.T. Borchardt, Hydrogen bonding potential as a determinant of the in vitro and in situ blood–brain barrier permeability of peptides, Pharm. Res. An Off. J. Am. Assoc. Pharm. Sci. 11 (1994) 412–419.
[22] M.F. Salvatore, Y. Ai, B. Fischer, A.M. Zhang, R.C. Grondin, Z. Zhang, G. A. Gerhardt, D.M. Gash, Point source concentration of GDNF may explain failure of phase II clinical trial, Exp. Neurol. 202 (2006) 497–505.
[23] K. Hynynen, Focused ultrasound for blood-brain disruption and delivery of therapeutic molecules into the brain, Exp. Opin. Drug Deliv. 4 (2007) 27–35.
[24] M. Kinoshita, N. McDannold, F.A. Jolesz, K. Hynynen, Noninvasive localized delivery of Herceptin to the mouse brain by MRI-guided focused ultrasound-induced blood-brain barrier disruption, Proc. Natl. Acad. Sci. U. S. A. 103 (2006) 11719–11723.
[25] M. Kinoshita, N. McDannold, F.A. Jolesz, K. Hynynen, Targeted delivery of antibodies through the blood-brain barrier by MRI-guided focused ultrasound, Biochem. Biophys. Res. Commun. 340 (2006) 1085–1090.
[26] F.Y. Yang, H.E. Wang, R.S. Liu, M.C. Teng, J.J. Li, M. Lu, M.C. Wei, T.T. Wong, Pharmacokinetic analysis of 111In-labeled liposomal doxorubicin in murine glioblastoma after blood-brain barrier disruption by focused ultrasound, PLoS One 7 (9) (2012) e45468.
[27] L.H. Treat, N. McDannold, N. Vykhodtseva, Y. Zhang, K. Tam, K. Hynynen, Targeted delivery of doxorubicin to the rat brain at therapeutic levels using MRI-guided focused ultrasound, Int. J. Cancer 121 (4) (2007) 901–907.
[28] L.H. Treat, N. McDannold, Y. Zhang, N. Vykhodtseva, K. Hynynen, Improved anti-tumor effect of liposomal doxorubicin after targeted blood-brain barrier disruption by MRI-guided focused ultrasound in rat glioma, Ultrasound Med. Biol. 38 (10) (2012) 1716–1725.

[29] Y. Shen, J. Guo, G. Chen, C.T. Chin, X. Chen, J. Chen, F. Wang, S. Chen, G. Dan, Delivery of liposomes with different sizes to mice brain after sonication by focused ultrasound in the presence of microbubbles, Ultrasound Med. Biol. 42 (2016) 1499–1511.
[30] Y. Shen, Z. Pi, F. Yan, C.K. Yeh, X. Zeng, X. Diao, Y. Hu, S. Chen, X. Chen, H. Zheng, Enhanced delivery of paclitaxel liposomes using focused ultrasound with microbubbles for treating nude mice bearing intracranial glioblastoma xenografts, Int. J. Nanomedicine 12 (2017) 5613–5629.
[31] A. Papachristodoulou, R.D. Signorell, B. Werner, D. Brambilla, P. Luciani, M. Cavusoglu, J. Grandjean, M. Silginer, M. Rudin, E. Martin, M. Weller, P. Roth, J. C. Leroux, Chemotherapy sensitization of glioblastoma by focused ultrasound-mediated delivery of therapeutic liposomes, J. Control. Release 295 (2019) 130–139.
[32] J.N. May, S.K. Golombek, M. Baues, A. Dasgupta, N. Drude, A. Rix, D. Rommel, S. Von Stillfried, L. Appold, R. Pola, M. Pechar, L. Van Bloois, G. Storm, A.J. C. Kuehne, F. Gremse, B. Theek, F. Kiessling, T. Lammers, Multimodal and multiscale optical imaging of nanomedicine delivery across the blood-brain barrier upon sonopermeation, Theranostics 10 (2020) 1948–1959.
[33] Q. Lin, K.L. Mao, F.R. Tian, J.J. Yang, P.P. Chen, J. Xu, Z.L. Fan, Y.P. Zhao, W.F. Li, L. Zheng, Y.Z. Zhao, C.T. Lu, Brain tumor-targeted delivery and therapy by focused ultrasound introduced doxorubicin-loaded cationic liposomes, Cancer Chemother. Pharmacol. 77 (2016) 269–280.
[34] C.Y. Lin, C.H. Tsai, L.Y. Feng, W.Y. Chai, C.J. Lin, C.Y. Huang, K.C. Wei, C.K. Yeh, C.M. Chen, H.L. Liu, Focused ultrasound-induced blood brain-barrier opening enhanced vascular permeability for GDNF delivery in Huntington's disease mouse model, Brain Stimul. 12 (2019) 1143–1150.
[35] C.Y. Lin, H.Y. Hsieh, W.G. Pitt, C.Y. Huang, I.C. Tseng, C.K. Yeh, K.C. Wei, H.L. Liu, Focused ultrasound-induced blood-brain barrier opening for non-viral, non-invasive, and targeted gene delivery, J. Control. Release 212 (2015) 1–9.
[36] J. Guo, G. Chen, J. Wu, C.T. Chin, Y. Shen, J. Chen, Y. Suo, Passive delivery of liposomes to mouse brain after blood-brain barrier opening induced by focused ultrasound with microbubbles, in: 2015 IEEE International Ultrasonics Symposium, IUS 2015, 2015.
[37] M. Aryal, I. Papademetriou, Y.Z. Zhang, C. Power, N. McDannold, T. Porter, MRI monitoring and quantification of ultrasound-mediated delivery of liposomes dually labeled with gadolinium and fluorophore through the blood-brain barrier, Ultrasound Med. Biol. 45 (2019) 1733–1742.
[38] M. Aryal, N. Vykhodtseva, Y.Z. Zhang, N. McDannold, Multiple sessions of liposomal doxorubicin delivery via focused ultrasound mediated blood-brain barrier disruption: a safety study, J. Control. Release 204 (2015) 60–69.
[39] M. Aryal, N. Vykhodtseva, Y.Z. Zhang, J. Park, N. McDannold, Multiple treatments with liposomal doxorubicin and ultrasound-induced disruption of blood-tumor and blood-brain barriers improve outcomes in a rat glioma model, J. Control. Release 169 (2013) 103–111.
[40] Z. Kovacs, P. Luciani, P. Roth, J.-C. Leroux, E. Martin, B. Wemer, Blood-brain barrier opening-based local delivery of 80 nm-sized liposomes in mice using pulsed focused ultrasound, J. Ther. Ultrasound 3 (2015) P24.
[41] H. Chen, E.E. Konofagou, The size of blood-brain barrier opening induced by focused ultrasound is dictated by the acoustic pressure, J. Cereb. Blood Flow Metab. 34 (2014) 1197–1204.
[42] B. Marty, B. Larrat, M. Van Landeghem, C. Robic, P. Robert, M. Port, D. Le Bihan, M. Pernot, M. Tanter, F. Lethimonnier, S. Mériaux, Dynamic study of blood-brain barrier closure after its disruption using ultrasound: a quantitative analysis, J. Cereb. Blood Flow Metab. 32 (2012) 1948–1958.
[43] S.V. Morse, A.N. Pouliopoulos, T.G. Chan, M.J. Copping, J. Lin, N.J. Long, J. J. Choi, Rapid short-pulse ultrasound delivers drugs uniformly across the murine blood-brain barrier with negligible disruption, Radiology 291 (2) (2019) 459–466.
[44] A.N. Pouliopoulos, S. Bonaccorsi, J.J. Choi, Exploiting flow to control the in vitro spatiotemporal distribution of microbubble-seeded acoustic cavitation activity in ultrasound therapy, Phys. Med. Biol. 59 (2014) 6941–6957.
[45] A.N. Pouliopoulos, C. Li, M. Tinguely, V. Garbin, M.-X. Tang, J.J. Choi, Rapid short-pulse sequences enhance the spatiotemporal uniformity of acoustically driven microbubble activity during flow conditions, J. Acoust. Soc. Am. 140 (2016) 2469–2480.
[46] J.J. Choi, M. Pernot, S.A. Small, E.E. Konofagou, Noninvasive, transcranial and localized opening of the blood-brain barrier using focused ultrasound in mice, Ultrasound Med. Biol. 33 (2007) 95–104.
[47] J.J. Choi, K. Selert, F. Vlachos, A. Wong, E.E. Konofagou, Noninvasive and localized neuronal delivery using short ultrasonic pulses and microbubbles, Proc. Natl. Acad. Sci. U. S. A. 108 (2011) 16539–16544.
[48] T.J. Collins, ImageJ for microscopy, Biotechniques 43 (2007) S25–S30.
[49] Honig MG, Hume RI. Fluorescent carbocyanine dyes allow living neurons of identified origin to be studied in long-term cultures.
[50] R. Münter, K. Kristensen, D. Pedersbæk, J.B. Larsen, J.B. Simonsen, T.L. Andresen, Dissociation of fluorescently labeled lipids from liposomes in biological environments challenges the interpretation of uptake studies, Nanoscale 10 (2018) 22720–22724.
[51] S. Snipstad, S. Hak, H. Baghirov, E. Sulheim, Ý. Mørch, S. Lélu, E. von Haartman, M. Bäck, K.P.R. Nilsson, A.S. Klymchenko, Davies C. de Lange, A.K.O. Åslund, Labeling nanoparticles: dye leakage and altered cellular uptake, Cytom. Part A 91 (2017) 760–766.
[52] R. Chopra, N. Vykhodtseva, K. Hynynen, Influence of exposure time and pressure amplitude on blood-brain-barrier opening using transcranial ultrasound exposures, ACS Chem. Neurosci. 1 (2010) 391–398.
[53] N. McDannold, N. Vykhodtseva, K. Hynynen, Effects of acoustic parameters and ultrasound contrast agent dose on focused-ultrasound induced blood-brain barrier disruption, Ultrasound Med. Biol. 34 (2008) 930–937.
[54] R.G. Thorne, C. Nicholson, In vivo diffusion analysis with quantum dots and dextrans predicts the width of brain extracellular space, Proc. Natl. Acad. Sci. U. S. A. 103 (2006) 5567–5572.
[55] P. Bilalis, L.A. Tziveleka, S. Varlas, H. Iatrou, pH-Sensitive nanogates based on poly (l-histidine) for controlled drug release from mesoporous silica nanoparticles, Polym. Chem. 7 (2016) 1475–1485.
[56] H.M.E. Azzazy, K. Hong, M.C. Wu, G.W. Gross, Interaction of cationic liposomes with cells of electrically active neuronal networks in culture, Brain Res. 695 (1995) 231–236.
[57] A. Lakkaraju, Y.E. Rahman, J.M. Dubinsky, Low-density lipoprotein receptor-related protein mediates the endocytosis of anionic liposomes in neurons, J. Biol. Chem. 277 (2002) 15085–15092.
[58] S. Lee, A.T. Ashizawa, K.S. Kim, D.J. Falk, L. Notterpek, Liposomes to target peripheral neurons and Schwann cells, PLoS One 8 (2013).
[59] Z. Chu, Y. Sun, C.Y. Kuan, G.A. Grabowski, X. Qi, C. Saposin, Neuronal effect and CNS delivery by liposomes, Ann. N. Y. Acad. Sci. 1053 (2005) 237–246.
[60] I.E. Thunnissen, E. Marani, W.J. Rietveld, "Homing" of Lucifer Yellow liposomes into hypothalamic neurons: a combined neuroanatomical Golgi and tracing technique, J. Neurosci. Methods 12 (1984) 113–123.
[61] S. Hashioka, Y.H. Han, S. Fujii, T. Kato, A. Monji, H. Utsumi, M. Sawada, H. Nakanishi, S. Kanba, Phosphatidylserine and phosphatidylcholine-containing liposomes inhibit amyloid β and interferon-γ-induced microglial activation, Free Radic. Biol. Med. 42 (2007) 945–954.
[62] S. Hashioka, Y.H. Han, S. Fujii, T. Kato, A. Monji, H. Utsumi, M. Sawada, H. Nakanishi, S. Kanba, Phospholipids modulate superoxide and nitric oxide production by lipopolysaccharide and phorbol 12-myristate-13-acetate-activated microglia, Neurochem. Int. 50 (2007) 499–506.
[63] N.J. Wiley, A.B. Madhankumar, R.M. Mitchell, E.B. Neely, E. Rizk, G.L. Douds, Z. Simmons, J.R. Connor, Lipopolysaccharide modified liposomes for amyotropic lateral sclerosis therapy: efficacy in SOD1 mouse model, Adv. Nanopart. 01 (2012) 44–53.
[64] G.W. Kreutzberg, Microglia: a sensor for pathological events in the CNS, Trends Neurosci. 19 (1996) 312–318.
[65] K. Nakajima, S. Kohsaka, Microglia: activation and their significance in the central nervous system, J. Biochem. 130 (2) (2001) 169–175.
[66] Rodrigues B. dos Santos, H. Oue, A. Banerjee, T. Kanekiyo, J. Singh, Dual functionalized liposome-mediated gene delivery across triple co-culture blood brain barrier model and specific in vivo neuronal transfection, J. Control. Release 286 (2018) 264–278.
[67] P. Madhusudanan, S. Reade, S.A. Shankarappa, Neuroglia as targets for drug delivery systems: a review, Nanomedicine 13 (2017) 667–679.
[68] F. Zhang, Y.A. Lin, S. Kannan, R.M. Kannan, Targeting specific cells in the brain with nanomedicines for CNS therapies, J. Control. Release 240 (2016) 212–226.
[69] R. Schmidt-Kastner, K. Wietasch, H. Weigel, U.T. Eysel, Immunohistochemical staining for glial fibrillary acidic protein (GFAP) after deafferentation or ischemic infarction in rat visual system: features of reactive and damaged astrocytes, Int. J. Dev. Neurosci. 11 (1993) 157–174.
[70] S.A. Liddelow, B.A. Barres, Reactive astrocytes: production, function, and therapeutic potential, Immunity 46 (2017) 957–967.
[71] D.F. Baban, L.W. Seymour, Control of tumour vascular permeability, Adv. Drug Deliv. Rev. 34 (1998) 109–119.
[72] Y. Boucher, H. Salehi, B. Witwer, G. Harsh, R. Jain, Interstitial fluid pressure in intracranial tumours in patients and in rodents, Br. J. Cancer 75 (1997) 829–836.
[73] A. Schroeder, J. Kost, Y. Barenholz, Ultrasound, liposomes, and drug delivery: principles for using ultrasound to control the release of drugs from liposomes, Chem. Phys. Lipids 162 (2009) 1–16.
[74] M.B.C. De Matos, R. Deckers, B. Van Elburg, G. Lajoinie, B.S. De Miranda, M. Versluis, R. Schiffelers, R.J. Kok, Ultrasound-sensitive liposomes for triggered macromolecular drug delivery: formulation and in vitro characterization, Front. Pharmacol. 10 (2019).
[75] S. Dromi, V. Frenkel, A. Luk, B. Traughber, M. Angstadt, M. Bur, J. Poff, J. Xie, S. K. Libutti, K.C.P. Li, B.J. Wood, Pulsed-high intensity focused ultrasound and low temperature - sensitive liposomes for enhanced targeted drug delivery and antitumor effect, Clin. Cancer Res. 13 (2007) 2722–2727.